Egypt. J. Chem. **Vol. 66**, No. 9 pp. 563 - 579 (2023)

Egyptian Journal of Chemistry

http://ejchem.journals.ekb.eg/

Quantification of domestic lead in daily used products using Pb-ceftriaxone/multiwalled carbon nanotube modified sensor and quantum calculations by density functional theory and non-linear optical properties

Ahmed F.A. Youssef[a,b]*, Yousry M. Issa[a], Samir A. Abdel-Latif[c], Heba Sherief [d], Sabrein H. Mohamed[a,e]

[a]*Chemistry Department, Faculty of Science, Cairo University, Giza, 12613, Egypt.*
[b]*University of Science and Technology, Zewail City, Giza, 12578, Egypt.*
[c]*Chemistry Department, Faculty of Science, Helwan University, 11795, Cairo, Egypt,*
[d]*Banknote Printing House, Central Bank of Egypt, Pyramid Street, Giza, Egypt.*
[e]*Chemistry Department, College of Science, Jouf University, P.O. Box 2014, Sakaka, Saudi Arabia.*

Abstract

A carbon paste electrode modified with Pb-Ceftriaxone and a multi-wall carbon nanotube was constructed. It showed Nernstian response to Pb(II), 30.42 mV/decade, over the concentration range 6.28×10^{-7}-1.29×10^{-3} mol L^{-1}, the detection limit of 3.90×10^{-7} mol L^{-1}, in the pH range 1.5-5.8 with a response time of ≤10 s at 25 °C and 20 days lifetime. Moreover, a study of the relation between Pb(II) concentration in banknote paper and their withdrawal criteria (soiling, deterioration, and aging) from circulation was performed and it revealed a good relation. That means lead concentration can be used as a new criterion for banknote withdrawal using the proposed electrode. To investigate the type of bond in the newly prepared compound, Pb-Ceftriaxone, quantum mechanical calculations of energies and geometries were done using the density functional theory with Becke's three-parameter exchange functional approach, the Lee-Yang-Parr correlation functional (B3LYP) combined with 6.311G** used as basis set. The evaluation of the Highest Occupied Molecular Orbital (HOMO) and Lowest Unoccupied Molecular Orbital (LUMO) has been used to explain the charge transfer within the Ceftriaxone compound. Geometrical parameters, molecular electrostatic potential maps, and total electron density analyses of the combination have been carried out. Total static dipole moment, mean polarizability, anisotropy of the polarizability, and mean first-order hyperpolarizability have also been attained.

Keywords: Modified multiwalled carbon nanotube carbon paste electrode; Lead (II); Ceftriaxone complex; Potentiometry, DFT studies, NLO properties

1. Introduction

Carbon paste electrode (CPE) has excellent attention because of their stable response, renewability, low ohmic resistance, and no internal solutions to work are needed [1]. A chemically modified carbon paste electrode (CMCPE) is a well-known potentiometric sensor for determining various ions [2-4]. The advantage of nanotechnology and nanostructure materials includes modifying the surface of the electrode, enhancing the thermal, mechanical, and chemical stability, and having excellent electrical conductivity [5].

Carbon nanotube (CNT) is used in sensor fabrication as it has unique electronic, chemical, and mechanical properties. It is characterized by its electrochemical and chemical stabilities in aqueous and non-aqueous solutions and excellent electronic conductivity for electron transfer reactions. Single-wall (CNT) and multi-wall carbon nanotube (MWCNT) are also characterized by their high surface area and good electronic properties that help widely in applied electroanalytical studies [6].

*Corresponding author e-mail: ahyoussef@zewailcity.edu.eg ; afahmy@sci.cu.edu.eg. (A. F. A. Youssef)
Received date 2022-08-13; revised date 2022-11-29; accepted date 2022-12-17
DOI: 10.21608/EJCHEM.2022.156055.6754

Recently the environmental contamination due to uncontrolled industrial waste has increased. This may be due to the growth of industrial activities and the generation of electronic waste. Among these pollutants is lead which is involved in many industries such as alloys, paints, batteries, and radiation-shielding sheets. When Pb(II) accumulates in the blood, it causes abdominal cramps; attention deflects disorder, and brain damage [7]. Lead in paints and PVC children's toys is a significant public health concern. A review of the analysis of domestic lead in lead-based paints and children's PVC toys was presented by Njatia and Magutab [8].

Thousands of methods, based on different analytical techniques, had been developed for the determination of lead. Of these methods spectrophotometry [9 and 10], atomic absorption spectrometry [11], ICP-OES atomic emission spectrometry [12], dispersive liquid-liquid extraction [13], HPLC [14], differential pulse anodic stripping voltammetry [15] and potentiometry [16]. Lectures data showed that different types of chemically modified carbon-based sensors had been developed. Table 1 shows the composition of some of these sensors, their characterization, and their applications.

Ceftriaxone, scheme 1, is used for the treatment of various infections with Salmonella typhi and Neisseria gonorrhoeae. Also, it can be used as an intramuscular injection or intravenous for outpatients pharmacologically [28].

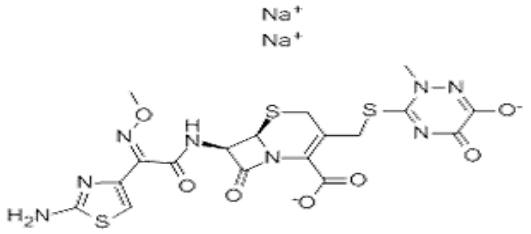

Scheme 1. Chemical structure of ceftriaxone sodium
One of the most daily used products is banknotes.

Some studies indicated that banknote papers might contain metal ions with different concentration levels. Until now, no studies considered whether we have a

Table 1. Data of some previously published CMCPE for determination of lead (II).

Ion-recognition element (CPEs)	Slope mV decade $^{-1}$	Sample	LOD, mol L^{-1}	Linear range, mol L^{-1}	Response time, s	Ref.
Nanosilica	29.80±0.2	Wastewater and black tea samples.	7.3×10^{-8}	1.0×10^{-7}-1.0×10^{-2}	10	17
2, 2'- (ethane 1, 2-diylbis (azanylylidene)) bis (ethan-1- yl-1- ylidene)) diphenol (L)	30.70±1.56	Water samples	1.5×10^{-7}	3.7×10^{-7}-1.0×10^{-2}	<14	18
2-((6-(5-bromo-2-hydroxybenzylideneamino) hexylimino) methyl)-4-bromophenol (BHBAHMBP)	29.50	Soil, tea and coffee samples	2.5×10^{-7}	5.0×10^{-7}-1.0×10^{-1}	~ 40	19
Thiosalicylamide-functionalized polysiloxane	28.10±0.2	Miscellaneous samples such as water and commercial lipsticks.	8.7×10^{-7}	4.3×10^{-6}-1.0×10^{-2}	~5	20
Pyridine para styrene sulfonamide and MWCNTs	29.43±0.3	Wastewater samples	6.0×10^{-9}	1.0×10^{-8}-1.0×10^{-1}	20	21
1,3-bis[2-(N-morpholino)acetamidophenoxy]propane (BMAPP)	29.96±0.34	Water samples	3.0×10^{-8}	5×10^{-8}-1×10^{-1}	<10	22
Dipyridile amine and MWCNTs	28.90	Water, soil, and plant samples	7.0×10^{-8}	9.5×10^{-8}-2.5×10^{-3}	50	23
1,1′-thiobis(naphthalene-2,1-diyl)bis(2-aminobenzoate) (TNBA)	29.00 ± 0.2	Water samples	5.0×10^{-8}	8.0×10^{-8}-1.0×10^{-2}	8	24
modified core/shell SiO_2/Fe_3O_4 nano-structure	29.84 ± 0.10	Various water, petrochemical wastewater and biological samples	$1.0\times10^{-9.02}$	2.5×10^{-9}-1.0×10^{-1}	5	25
(N-(4- hydroxyphenyl) ethanamide) and MWCNTs	29.73	Water samples	7.5×10^{-9}	1.0×10^{-8}-1.0×10^{-1}	25	26
2-aminothiophenol grafted MWCNTs (L-g-MWCNTS)	29.50	Soil, wastewater, lead accumulator waste, and black tea samples	3.2×10^{-10}	5.9×10^{-10}-1.0×10^{-2}	25	27

relation between the banknote circulation lifetime and the metal ion concentrations. The banknote withdrawal criteria are based on soiling, deterioration, and aging. Metal or heavy metal ions, which are health factor, are not listed in these criteria [29].

Based on the adverse health effect of domestic lead, the aim of the current study is its quantification in diverse environment such as children's toys, cosmetics, food, accessories, and currency samples by using a homemade chemically modified carbon paste electrode (CMCP) based on Pb-Ceftriaxone (Pb-CFT) as an electroactive material enhanced with MWCNT as additive. A deeper study is required to understand the relation between the banknote metal ion concentration, Pb(II) ion, and its lifetime in circulation expressed as banknote fitness level.

Natural bond orbital analysis (NBO) has been utilized for charge transfer investigation or conjugate interaction in molecular systems and estimate inter- and intra-molecular interactions. Different quantum chemical parameters were calculated, such as bond angles, bond lengths, first-order hyperpolarizability (β), and electronic dipole moment (μ) using DFT-B3LYP/6-311G** level of calculation.

2. Experimental

2.1. Reagents and materials

Dibutyl-butyl phosphonate (DBBP), Bis (2-ethyl hexyl) phthalate (DOP), Dibutyl phthalate (DBP), Tributyl phosphate, Tricresyl phosphate (TCP), 2-Nitrophenyl phenyl ether, and graphite powder were purchased from Fluka Chemika company, Switzerland.

KNO_3, $NaNO_3$, HNO_3, $Mg(NO_3)_2.6H_2O$, $Ba(NO_3)_2$, $Ni(NO_3)_2.6H_2O$, NH_4NO_3, $Al(NO_3)_3.9H_2O$, $Bi(NO_3)_3$, ZnO, $Cu(NO_3)_2$, $Mn(NO_3)_2$, $Pb(NO_3)_2$ (95%), N-cetyl-N, N, trimethyl ammonium bromide, polyethylene glycol (PEG) with a molecular weight of 6000, Silver nitrate ($AgNO_3$), and Sodium hydroxide (NaOH) pellets were purchased from Aldrich chemical company, USA.

Carbon nanotube (particle size <50 nm and molecular weight: 12.01) from WINLAB (Laboratory chemicals reagents fine chemicals) and Fullerene, carbon nanotube, multi-walled, 0.1-10 micron long, 3-20 nm OD, 1-3 nm ID, 95% was purchased from Alfa Aesar (A Johnson Mattey company).

2.2. Solutions

For preparations of all experiments, deionized water was used. A stock solution of concentration 0.1 mol L^{-1} of lead nitrate solution was prepared by dissolving 1.656 g $Pb(NO_3)_2$ in 50 mL deionized water. For reservation to prevent hydrolysis and standardized by complexometric titration [30], two drops of 0.1 mol L^{-1} nitric acid were added.

For selectivity investigation of the proposed ion-selective electrodes, 0.1 mol L^{-1} salt solution of each of the following ions, Zn^{2+}, Na^{+}, K^{+}, Mg^{2+}, Ni^{2+}, NH_4^{+}, Ba^{2+}, Al^{3+}, Cu^{2+}, Mn^{2+}, and Bi^{2+} were prepared.

2.3. Apparatus

JANEWAY 3010 digital pH/mV meter was applied for potential measurements. Sigma Aldrich Ag/AgCl (3M KCl) electrode was used as a reference electrode, and for obtaining the deionized water, Millipore Elix S (Automatic Sanitization Module) (ASM) was used.

For lead ion determination in actual samples, Agilent 5100 Synchronous Vertical Dual View (SVDV) ICP-OES, with Agilent Vapor Generation Accessory VGA 77 was used. The National Institute of Research performed the measurements.

The surface morphology of the electrodes was investigated for high-resolution imaging using Scanning Electron Microscope (SEM) (QUANTA FEG 250), Detector BSED, HV (20.00 Kv), and HFW 16.6 μm. Also, for the quantitative analysis on the sample surface Energy-Dispersive X-ray (EDAX) HV (20.00 Kv), magnification: 240000, live Time (s): 30, takeoff: 34, Resolution (eV): 122.8 and amp Time (μs): 3.84 were used. Both SEM and EDX were performed at the National Institute of Research.

2.4. Preparation of lead and silver nanoparticles

An exact amount of Polyethylene glycol (PEG), 20 g, was weighed and dissolved in one Liter of the Reverse Osmosis (RO) purified water and then heated up to 50°C. To dissolve the PEG completely, the solution was stirred for another 1 hour and to remove impurities, the PEG solution obtained was then filtered. For the preparation of nanosized particles, 0.5 g of silver nitrate and lead nitrate was weighed and added to the prepared PEG solution at a constant temperature of 50°C and the stirring rate which was continued for 1 hour, and after particle formation,

filtration was performed to the solution; then, the particles were rinsed with RO water many times. The particles were washed finally with ethanol. Then drying of particles was conducted in the oven at 60°C for overnight. To confirm the chemical compound composition, crystallographic structure, and the size distribution measurement, Zeta sizer Nano series, Fourier transform infrared spectroscopy (FT-IR) and X-ray diffraction (XRD) analysis studies were employed [31].

2.5. Preparation of lead-ceftriaxone complex

A 10 mL solution of 1 mmol $Pb(NO_3)_2$ was added to a 10 mL solution of 2.0 mmol ceftriaxone sodium, where brown precipitate was obtained. The residue was washed many times with deionized water, filtered off, and finally air-dried.

2.6. Preparation of modified carbon paste electrodes

A chemically modified carbon paste electrode (CMCPE) was prepared by thoroughly mixing weighed amounts of the complex with TCP and high-purity graphite until obtaining a uniformly wetted paste. The mixture was then packed at the end of a Teflon holder of 12.0 cm in length with a hole at one end of 3.5 mm deep and 7.0 mm diameter. An electrical contact was obtained by a stainless-steel rod through the middle of the holder then the paste was smoothened onto paper and used directly without pre-conditioning requirements for potentiometric measurements [32]. According to the subsequent cell assembly, all EMF measurements were carried out: Ag//AgCl, KCl (3.0 mol L^{-1}) // test solution //filling modified carbon paste // carbon paste electrode.

For investigation of the electrode's performance, the EMFs of the Pb(II) solutions were measured in a range of different concentrations of 1.0×10^{-8} to 1.0×10^{-1} mol L^{-1} [33]. For the calibration graphs' construction, the addition of suitable increments of standard Pb(II) solutions to 50 mL deionized water was done in order to cover the whole working concentration range 1.39×10^{-8} - 2.79×10^{-2} mol $L^{-1.}$ The CMCP electrode and reference electrode were immersed in the solution. Values of emf were recorded after each addition at 25±l ºC and then plotted versus the negative logarithmic of the ion concentration.

2.7. Nature of plasticizer

The plasticizer is very important for optimizing the performance of CPEs by influencing the dielectric constant of the paste. Seven plasticizers of different polarities were used (DOP), (DBBP), (TCP), (DOA), (DBP), Bis (2-ethyl hexyl)-sebacate (EHS), and 2-Nitro phenyl phenyl ether (NPPE) in order to the study of the effect of plasticizer on the selective response of the Pb(II) ISEs.

2.8. Effect of pH

The dependence of the potentiometric response of the proposed electrode on the pH value of the Pb(II) solution was studied at three concentration levels (1.0×10^{-5}, 1.0×10^{-4}, and 1.0×10^{-3} mol L^{-1}) over a pH range between 1.0 and 9.0.

2.9. Effect of interfering ions

A study of the influence of some inorganic cations on the electrode's response was done graphically by plotting calibration curves for all tested ions and comparing them with the Pb(II) ion calibration curve. The matched potential method was applied to determine the selectivity coefficient [34] that doesn't depend on the Nicolsky-Eisenman equation or on its modifications. This method was recommended by IUPAC in 2002 [35] as a way that provides analytically relevant practical selectivity coefficient values.

2.10. Potentiometric determination

For the potentiometric determination, a standard addition method was applied, where a known gradual change was achieved by adding a standard solution to the sample. This was achieved by pure solutions of different concentrations ranging from 5.0×10^{-5} to 1.0×10^{-8} mol L^{-1} by adding known volumes of a Pb(II) standard solution to 100 mL water which contains different amounts of the Pb(II) samples. Also, the standard addition method was applied for actual examples, including indoor dust collected from air vacuum, outdoor dust collected from the street, Egyptian banknote of 1 Pound denomination of three different issuing dates (3, 7, and 18 months), American banknote of 1 Dollar denomination of 7 months in circulation, gum from a market, watercolors from a bookstore, toys, cosmetics, and accessories samples from a street vendor. For each addition, the change in mV reading was recorded and used to calculate the concentration of the Pb(II) in the sample solution using the following equation [36]:

$$C_x = C_s \left(\frac{V_s}{V_x + V_s}\right) \left(10^{n(\Delta E/S)} - \frac{V_x}{V_s + V_x}\right)^{-1}$$

C_x is regarded as the sample concentration to be determined, V_x is considered as the volume of the original sample solution, C_s and V_s are the concentration and volume of the standard solution added to the sample, respectively, S is considered as the slope of the calibration graph and ΔE is regarded as the potential change after the increment of a particular volume of a standard solution.

2.11. Sample preparation

All samples were digested to possess an acceptable matrix for measuring lead ions and to provide adequate and consistent recovery compatible with the analytical method (APHA, 2017) [37]. 0.2 g of each sample was added to a beaker, and concentrated HNO_3 acid was added until the sample was completely dissolved. Then, all samples were then heated to eliminate the organic matter and then transferred to a 25 mL volumetric flask after cooling, and deionized water was added to the mark followed by the addition of concentrated HNO_3 acid to adjust the pH value between 1.5-5.8. The amount of lead was measured by Agilent 5100 Synchronous Vertical Dual View (SVDV) ICP-OES with Agilent Vapor Generation Accessory VGA 77 and by the proposed lead selective electrode.

2.12. Morphology of the surface

To investigate the change in surface morphology of the electrode compared with composition, three electrodes of different compositions were prepared (a) unmodified CPE with a composition of 50.0% graphite and 50.0% TCP. (b) modified CPE with composition 2.0% Pb-CFT, 49.0% Graphite, and 49.0% TCP and (c) modified CPE after the addition of MWCNTs with composition 2.0% Pb-CFT, 48.5% Graphite, 48.5% TCP and 1.0% MWCNTs. SEM and EDX techniques were used to confirm the change in the surface composition.

2.13. Study of the criteria of banknote withdrawal from circulation

Random samples, 500 notes of denomination 5 LE, were selected from circulation and sorted visually to five levels from 1 to 5 according to fitness perspective (soiling, deterioration, and aging) from the newest level to the oldest one. Another level was used which is zero fitness level which represents a new banknote (uncirculated).

Study of the withdrawal reasons involved measurement of (i) brightness by using Elrepho type Spectrophotometer under D65 illumination at the watermark area as it is the clearest area in the banknote, (ii) stiffness, which expresses deterioration according to ISO 2493 specification, by using bending resistance tester in millinewton (mN), where the cross direction was chosen to measure because the available size was the note size height (7 mm), and (iii) Porosity, which express aging, by using Bentsen porosity tester which measures the rate of airflow between fibers in mL/min by forcing air through the banknote. An area away from the watermark and thread was chosen at a straight surface for the porosity test.

The percentage of the population with different fitness levels was calculated for soiling, deterioration, and aging and repeated for 5 different issuing years continuously to find the fitness level at which the Central Bank of Egypt withdraws banknotes from circulation. All tests were done in the Research and Development and Quality Control Laboratory in the Banknote Printing House, Central Bank of Egypt.

The lead concentration was measured in the new banknote and in the circulated banknote at three different fitness levels 1, 3, and 5 which correspond to 3, 7, and 18 months in circulation, respectively. Measurements were performed potentiometrically by the proposed electrode, Pb-CFT, and by the atomic spectral techniques, ICP-OES.

2.14. Computational details

To attain the molecular conformation of a Ceftriaxone compound, and due to the absence of single-crystal X-ray structure analysis, energy minimization analyses were done employing the Gaussian-09W software package [38]. The ground state geometrical structure of the ceftriaxone compound was optimized using the DFT method [39] with the B3 exchange-correlation functional approach [40]. The basis set 6-311G** for C, H, N, and S atoms was applied [41]. The geometry of the investigated systems was optimized for the gas phase without any symmetry constraints. Gauss View 5 software [42] was used to create figures of molecular orbitals (MOs). The quantum chemical parameters of the studied compounds were obtained from the calculations as energies of the highest occupied molecular orbital (EHOMO), the lowest unoccupied molecular orbital (ELUMO), HOMO-LUMO energy gap, Eg, chemical potentials, absolute electronegativities, χ, π absolute hardness, η, global electrophilicity, ω, global softness, S, and additional electronic charge, ΔN_{max}. These parameters were calculated using the following

equations [43, 44]; Eg = ELUMO – EHOMO, χ = -EHOMO + ELUMO/2, η = ELUMO – EHOMO/2, σ =1/η, π = -χ, S = 1/2η, $\omega = \pi^2/2\eta$ and $\Delta N_{max.} = -\pi/\eta$. The spin density difference map calculations were achieved to investigate their optical properties. Natural bond orbital (NBO) calculations [45] with the NBO code in Gaussian 09 were done to understand the different second-order interactions between the filled orbital of one subsystem and the empty orbital of another subsystem, that is the calculation of the molecular delocalization or hyperconjugation. The total static dipole moment (μ), the mean polarizability $\langle\alpha\rangle$, the anisotropy of the polarizability, $\Delta\alpha$, and the mean first-order hyperpolarizability, $\langle\beta\rangle$ using the x, y, z components were also calculated using the following equations at B3LYP/ 6-311G** level of theory: [46-48]

$$\mu = (\mu^2_x + \mu^2_y + \mu^2_z)^{1/2},$$

$$\langle\alpha\rangle = 1/3\ (\alpha_{xx} + \alpha_{yy} + \alpha_{zz}),$$

$$\Delta\alpha = ((\alpha_{xx} - \alpha_{yy})^2 + (\alpha_{yy} - \alpha_{zz})^2 + (\alpha_{zz} - \alpha_{xx})^2/2)^{1/2},$$

$$\langle\beta\rangle = (\beta^2_x + \beta^2_y + \beta^2_z)^{1/2},$$

Where,

$$\beta_x = \beta_{xxx} + \beta_{xyy} + \beta_{xzz},$$

$$\beta_y = \beta_{yyy} + \beta_{xxy} + \beta_{yzz},$$

$$\beta_z = \beta_{zzz} + \beta_{xxz} + \beta_{yyz}.$$

3. Results and discussion

3.1. Effect of composition

The carbon paste composition and the nature of the modifier affect significantly the selectivity and sensitivity of the electrode. Thus, the effect of the amounts of Pb-CFT present in the carbon paste was investigated. Investigation of potential response was done within a concentration range of 1.0×10^{-8} - 1.0×10^{-1} mol L^{-1} of all potentiometric carbon paste electrodes as a function of the Pb(II) activity.

The best electrode composition was 2.0% Pb-CFT and 49% DOP as a plasticizer as it shows a Nernstian slope, 28.87 mV, and has a lower detection limit of 1.95×10^{-6} mol L^{-1} and a more comprehensive concentration range of 6.32×10^{-6}-3.32×10^{-3} mol L^{-1} than the other examined compositions Table 2. The ion-selective electrode response has been attributed to an exchange process of Pb(II) ions between the analyzed solution and the mediator. The system equilibrium was achieved when the electrochemical potential of Pb(II) ions were equal within the two phases, and the Pb(II) ions in the aqueous phase do not influence the activity of the ions in the organic phase [49].

3.2. Effect of plasticizer and additive

The nature of the plasticizer plays an essential role in determining the characteristics of the electrode as it affects the dielectric constant of the paste phase and the mobility of the ionophore molecules. A good plasticizer should have a high lipophilicity, high molecular weight, and a low tendency for exudation from the paste matrix. The influence of plasticizer type on the properties of the Pb(II) chemically modified carbon paste electrode, Pb-CFT, was investigated using seven solvents with different polarities (DOP), (DBBP), (TCP), (DOA), (DBP), Bis (2-ethyl hexyl)-sebacate (EHS) and 2-Nitro phenyl phenyl ether (NPPE). EHS and DOP electrodes (Nos. 11 and 12) gave a near-Nernstian response of slopes 27.80 and 27.87 mV/decade respectively over the concentration ranges, 1.15×10^{-4} - 1.29×10^{-3} and 6.32×10^{-6}- 3.32×10^{-3} mol L^{-1}, respectively, and detection limit values of 1.03×10^{-5} and 1.95×10^{-6} mol L^{-1}. The paste with the DBP (No. 7) as solvent mediator had the worst response towards lead as the slope was 10.81 mV/decade and the detection limit was 3.00×10^{-5} mol L^{-1}. Although 2-Nitro phenyl phenyl ether (NPPE) has a high polarity, it increased the slope and detection limit to 58.40 mV/decade and 4.06×10^{-5} mol L^{-1}, respectively, while decreasing the linearity concentration range to 1.15×10^{-4}- 1.24×10^{-2} mol L^{-1}.

The Pb(II)-CMCPE with TCP as a solvent mediator exhibits the best response in which it has a slope of 28.70 mV/decade and detection limit of 3.90×10^{-7} mol L^{-1}. This can be due to the high molecular weight, high lipophilicity, and low dielectric constant of this plasticizer which enables mobility and solvation of complex through the paste.

It is known that the potentiometric behavior of a specific ion-selective electrode can be improved by additives by improving the response behavior and selectivity and reducing the ohmic resistance [50, 51]. Thus, the effect of CNT, N-Cetyl-N, N, N, trimethyl ammonium bromide (NCTAB), MWCNT, PbNPs, and AgNPs were studied; Table 2.

Table 2. Performance characteristics of Pb-CFT CMCPE at 25°C±1.

Paste No.	Composition %					Slope (mV/decade) ±S.E*	LOD (mol L^{-1})	Linear range (mol mL^{-1})
	Plasticizer		Reagent %	Graphite %	Additive %			
	%	Name						
1	49.5		1	49.5	-	34.28± 0.50	1.01×10^{-6}	1.95×10^{-6}- 3.32×10^{-3}
2	49.0		2	49.0	-	28.87± 0.66	1.95×10^{-6}	6.32×10^{-6}- 3.32×10^{-3}
3	48.5	**DOP**	3	48.5	-	26.25± 1.10	1.95×10^{-6}	2.54×10^{-6}- 1.24×10^{-2}
4	48.0		4	48.0	-	26.12± 0.98	2.54×10^{-6}	6.32×10^{-6}- 3.32×10^{-3}
5	47.5		5	47.5	-	24.31± 0.76	2.54×10^{-6}	4.01×10^{-6}- 2.11×10^{-3}
6		**TCP**			-	28.70± 1.55	3.90×10^{-7}	6.28×10^{-7}- 6.09×10^{-4}
7		**DBP**			-	10.81± 0.56	3.00×10^{-5}	4.70×10^{-5}- 9.11×10^{-4}
8		**DBBP**			-	20.73± 0.96	9.66×10^{-6}	1.31×10^{-5}- 1.87×10^{-2}
9	49.0	**DBA**	2	49.0	-	52.82± 1.34	4.06×10^{-5}	1.15×10^{-4}- 1.87×10^{-2}
10		**NPPE**			-	58.43± 0.51	4.06×10^{-5}	1.15×10^{-4}- 1.24×10^{-2}
11		**EHS**			-	27.80± 0.67	1.03×10^{-5}	1.15×10^{-4}- 1.29×10^{-3}
12		**DOP**			-	28.87± 0.75	1.95×10^{-6}	6.32×10^{-6}- 3.32×10^{-3}
13					1% CNT[1]	35.76± 0.84	2.54×10^{-6}	6.32×10^{-6} - 1.29×10^{-3}
14					1% NCTAB[2]	9.80± 0.98	1.30×10^{-7}	3.93×10^{-7} -2.01×10^{-5}
15**	**48.0**	**TCP**	2	49.0	1% MWCNT[3]	30.42± 1.45	3.90×10^{-7}	6.28×10^{-7}-1.29×10^{-3}
16					1% PbNPs[4]	24.30± 0.84	4.01×10^{-6}	4.01×10^{-6}-1.29×10^{-3}
17					1% AgNPs[5]	28.27± 0.82	4.01×10^{-6}	6.32×10^{-6}- 1.24×10^{-2}

** 3 replicate measurements. ** Best composition*
1: Carbon Nano Tube 2: N-Cetyl-N, N, N, trimethyl Ammonium Bromide 3: Multi-walled Carbon Nano Tube
4: Lead Nano-sized particles 5: Silver Nano-sized particles

It was found that MWCNT improves the performance characteristics of the electrode (slope 30.42 mV/decade with detection limit of 3.90×10^{-7} mol L^{-1}, and linear range of 6.28×10^{-7}-1.29×10^{-3} mol L^{-1}) relative to the unmodified one that has a slope of 28.70 mV/decade with the same detection limit of 3.90×10^{-7} mol L^{-1}, and a linear range of 6.28×10^{-7}-6.09×10^{-4} mol L^{-1}.

3.3. Effect of pH

The effect of pH on the response of the Pb-CFT electrode was investigated with a series of Pb(II) solutions, 1.0×10^{-5}-1.0×10^{-3} mol L^{-1}. Small volumes of NaOH or HNO_3 from 0.1-1.0 mol L^{-1} were added to the test solutions to adjust the pH, and the variation in the potential was recorded. The results showed that the potential readings of the electrodes were nearly constant between pH 1.5-5.8, Fig. 1. The emf of the sensors decreased at pH >5.8 due to the precipitation of $Pb(OH)_2$, formation of hydroxyl lead complexes, and competition of OH^- ion with the complexes for Pb(II) ions. The potential readings increased at pH values lower than 1.5, due to the interference of hydronium ions. Lead hydroxide doesn't precipitate below this pH value due to the low concentrations of hydroxide ions in the work solution as the ionic product of lead hydroxide $Pb(OH)_2$ will be less than the solubility product no precipitate will be formed.

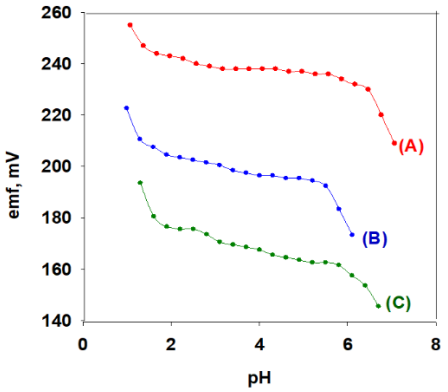

Fig. 1 Effect of pH on 1.0 (A), 0.1 (B), and 0.01 mmol L^{-1} (C) of lead (II) solution on the potential response of Pb-CFT based electrode.

3.4. Effect of temperature

Calibration graphs of p Pb(II) Vs. E electrode were constructed in order to study the thermal stability of the constructed electrodes at different temperatures of test solution within the range 25-55 °C as the potential of the CMCP-electrodes is affected by the temperature of the test solution. The usable concentration ranges and the electrode's slopes at different test solution temperatures are shown in table 3.

The ion-selective electrodes' potential is usually affected by the temperature of the test solution. Low thermal coefficient is characteristic for thermally

stable ion-selective electrode which reflects the good applicability of the electrode over a wide range of temperatures.

3.5. Response time

The concentration of Pb(II) solution was changed over the concentration range 1.0×10^{-6} - 1.0×10^{-1} mol L^{-1}, Fig. 2. and the reasonable response time was recorded. The results indicated that the entire concentration range of the paste electrodes reaches their equilibrium response in a brief time (≤10 s). This can be explained by the fast exchange kinetics of lead ion's complexation formation or decomplexation at the test solution-paste interface.

Table 3. Performance characteristics of Pb-CFT CMCPE at different test solution temperatures.

t, ºC	Slope (mV/decade)	Linear range (mol L^{-1})	LOD (mol L^{-1})	E^o elec. (mV)	E^o Cell (mV)
25	32.01± 0.86	$6.28x10^{-7}$-$2.11x10^{-3}$	6.30×10^{-7}	200	441.2
35	31.96± 0.57	$1.95x10^{-6}$-$2.11x10^{-3}$	1.48×10^{-6}	215	449.4
45	31.45± 1.45	$1.01x10^{-6}$-$9.11x10^{-4}$	1.95×10^{-6}	225	452.3
55	30.85± 1.24	$1.95x10^{-6}$-$9.11x10^{-4}$	3.20×10^{-6}	250	469.8

The standard cell potentials were determined from the respective calibration plots at different temperatures within the range under study to calculate the thermal coefficient of the cell $(dE^\circ/dt)_{cell}$ which is the intercept of these plots at pPb(II) = 0. Knowing that E^o_{cell} is related to (dE°/dt) by equation [52]:

$$E^o_{cell} = E^o_{25^\circ C} + (dE^o/dt)\ (t-25)$$

A straight line was produced from a plot of E^o_{cell} verses (t-25). The slope of this plot was taken as the thermal coefficient of the cell. The values of the standard potentials of electrodes ($E^o_{elec.}$) were calculated by subtracting the standard electrode potential of the silver/silver chloride electrode at different temperatures. The following correlation for the standard potential of the silver chloride electrode as a function of temperature was given by Bard et al. [53] (where t is the temperature in °C):

$$E^\circ(V) = 0.23695 - 4.8564\times10^{-4}\,t - 3.4205\times10^{-6}\,t^2 - 5.869\times10^{-9}\,t^3$$

for $0 < t < 95$ °C

The $E^\circ_{Ag/AgCl}$ (mV) values are 241.2, 234.4, 227.3, and 219.8 at temperatures 25, 35, 45, and 55 °C, respectively. After plotting a straight line between ($E^o_{elec.}$) versus (t-25) for each electrode, the slope of the line was recorded and taken as the thermal coefficient of the ion-selective electrode. The values of $(dE^o/dt)_{cell}$, and $(dE^o/dt)_{elec.}$ were 0.21×10^{-3} and 0.30×10^{-3}, respectively, which indicate the high thermal stability of the studied ion-selective electrodes for the wide temperature range and show no deviation from the theoretical Nernstian behavior.

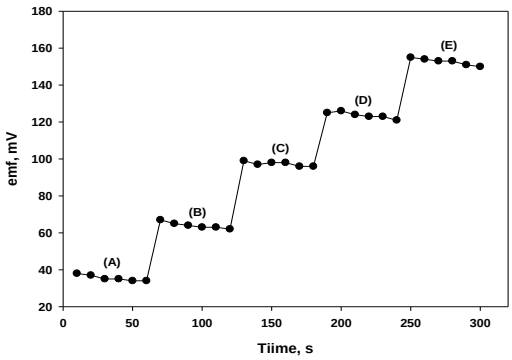

Fig 2. Potential-time plot for the response of Pb-CFT based electrode for step changes in concentration of Pb(II) solution: (A) $1.0x10^{-6}$, (B) $1.0x10^{-5}$, (C) $1.0x10^{-4}$, (D) $1.0x10^{-3}$ and (E) $1.0x10^{-2}$ mol L^{-1}.

3.6. Life span

The carbon paste electrodes' behavior and their changes through time is not often quoted. For a few special mixtures of more than one volatile binder (e.g., organic esters) [54, 55], it can be observed that they can desiccate within a few weeks, while other mixtures don't survive for more than 24 hours. Two experiments have been used for our investigated electrode based on 2.0% Pb-CFT, 48.5% TCP as a plasticizer, and 1.0% MWCNT. In the first experiment, the electrode was hung in the air without renewing the surface while in the second experiment, the electrode was soaked in 1.0×10^{-3} mol L^{-1} Pb(II)

solution. The electrode's response was measured periodically every 2-5 days. The results showed that the electrodes live for at least 20 days when hanged in the air without renewing the surface and 16 days when soaked in 1.0×10^{-3} mol L^{-1} Pb(II).

3.7. Selectivity

Selectivity is a measure of the extent of utility of any electrode in actual sample measurements. It represents the response of the ion-selective electrode for a primary ion in the presence of other ions within the same solution. For the selectivity coefficients evaluation of Pb-CFT towards many inorganic cations, the matched potential method was applied in which the selectivity coefficient $K^{MPM}_{Pb,,J}$ is given by:

$$K^{MPM}_{Pb,,J} = \frac{\Delta a_{pPb^{2+}}}{a_B} = \frac{a'_{pPb^{2+}} - a_{pPb^{2+}}}{a_B}$$

The selectivity coefficient can be determined by measuring the change in potential upon increasing the concentration of the primary ion activity (pPb(II)) by a definite amount from an initial value of $a_{pPb^{2+}}$ to $a'_{pPb^{2+}}$where, a_B represents the activity of the interfering ion added to the same reference solution of activity $a_{pPb^{2+}}$until it reaches the same potential change. The $K^{MPM}_{Pb,,J}$ values are in the range of 1.0×10^{-3} - 1.0×10^{-4}, and the activity of Pb(II) was taken as 1.0×10^{-5} mol L^{-1} as a reference solution in this study. This indicates that all ions tested exhibit little interference on the functioning of the proposed lead electrode. The potential response of the electrode was constructed at varying concentrations of these ions and compared to that of lead ion in Fig. 3. It is evident from the figures that there is no significant electrode response towards all foreign cations tested which confirms that the proposed sensor is highly selective to lead over many cations examined.

3.8. Analytical applications

Investigation of the lead concentration in different samples using the Pb-CFT as indicator electrode in the titrimetric determination of Pb(II) ion was done successfully in pure samples in concentrations ranging from 5.0×10^{-8} to 1.0×10^{-5} mol L^{-1}. The recovery ranges are between 98.67 and 103.56, Table 4.

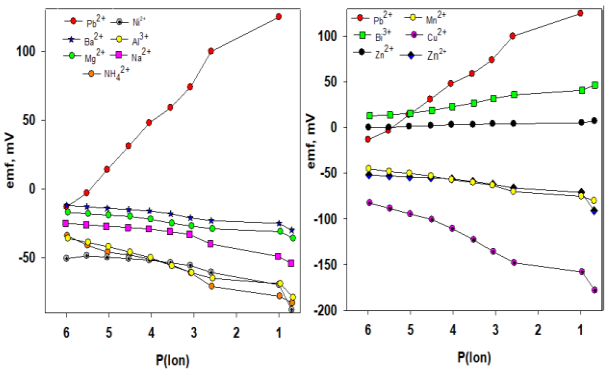

Fig. 3 Potential responses of Pb-CFT based electrode for different ions.

Table 4. Determination of lead in pure samples potentiometrically using the proposed Pb-CFT CMCPE.

Taken, mg Pb^{2+}	Recovery %±SD*	RSD %
10.63	103.40± 1.58	1.53
2.07	103.07± 3.15	3.06
1.04	100.12± 2.12	2.12
0.21	98.67± 3.28	3.33
0.10	100.92± 2.48	2.46
0.02	103.56± 2.14	2.07
0.01	100.26± 1.93	1.92
0.002	99.90± 2.37	2.38

Also, the proposed electrode was applied for lead determination in different environmental samples, including indoor dust collected from the air vacuum, outdoor dust collected from the street [56], Egyptian banknote as three samples of denomination 5 LE at three different fitness levels in circulation 1, 3 and 5 with issuing dates 3, 7 and 18 months, respectively. Also, American banknote of denomination 1 Dollar of 7 months lifetime in circulation, gum from the market, watercolors from a bookstore, toys, cosmetics, and accessories samples from street vendors are analyzed using the proposed electrode.

For all the previously mentioned samples, the standard addition method was applied for Pb(II) determination. The results given in table 3 shows a good agreement between the results obtained from the ICP-OES method and the proposed electrode with a recovery range between 96.89-101.74%, Table 5.

Table 5. Determination of lead ion in environmental samples, children toys, cosmetics, accessories, currency, and gum potentiometrically using the proposed Pb-CFT CMCPE compared to the ICP-OES.

Sample No.	Sample type	ICP method mg/L	Potentiometrically mg/L	Recovery% ±SD*	RSD%	F-test	t-test
1	Air dust	5.49	5.56	101.28± 2.81	2.79	1.45	1.60
2	Indoor dust	7.65	7.68	100.39± 2.40	2.39	0.92	1.36
3	Coin	5.57	5.53	99.28± 2.10	2.11	1.10	2.10
4	A banknote (3 months in circulation)	1.79	1.78	99.44± 3.13	3.16	1.80	1.45
5	A banknote (7 months in circulation)	5.73	5.69	99.30± 1.87	1.88	1.55	2.25
6	A banknote (18 months in circulation)	7.45	7.58	101.74± 1.70	1.67	1.28	0.86
7	Dollar (7 months in circulation)	7.42	7.35	99.06± 1.09	1.10	2.42	2.02
8	Toys	1.94	1.97	101.55± 0.81	0.80	1.58	1.56
9	Gum	46.37	47.03	101.42± 0.90	0.89	3.24	0.95
10	Watercolors	10.04	10.17	101.29± 0.57	0.56	2.65	1.55
11	Cosmetics	1.93	1.87	96.89± 1.51	1.56	1.35	3.14
12	Accessories	29.15	28.68	98.39± 1.26	1.28	1.31	1.02

For all the previously mentioned samples, the standard addition method was applied for Pb(II) determination. The results given in table 3 shows a good agreement between the results obtained from the ICP-OES method and the proposed electrode with a recovery range between 96.89-101.74%, Table 5.

The assay method for Pb(II) ions was achieved using three batches with five determinations for statistical treatment of results. F-tests and t-tests were used to compare the precision and accuracy of the employed method to those methods used as references [12, 57 and 58]. The results, Table 5, are lower than the tabulated ones, which indicate that the present method applying the newly developed electrode does not exhibit significant differences with those published. This reflects the accuracy and precision of the current process, Table 5.

3.9. Surface morphology study

To study the change in surface morphologies of the prepared membrane films, three different electrodes with different compositions were prepared (a) unmodified CPE with compositions 50.0% graphite and 50.0% TCP, (b) Modified CPE with compositions 2.0% Pb-CFT, 49.0% Graphite and 49.0% TCP and (c) Modified CPE after addition of MWCNTs with composition 2.0% Pb-CFT, 48.5% Graphite, 48.5% TCP and 1% MWCNTs. The results showed a clear difference between these electrodes which was confirmed by the SEM and EDX, Figs. 4-6

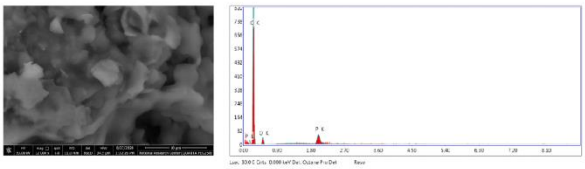

Representative element	Weight %	Atomic %	Net Interactive	Error %
C	88.26	90.19	108.53	6.13
O	11.18	8.78	5.58	18.36
P	256	1.04	14.26	11.07

Fig. 4 SEM-EDX of membrane films containing 50.0% Graphite and 50.0% TCP (total weight 20 mg).

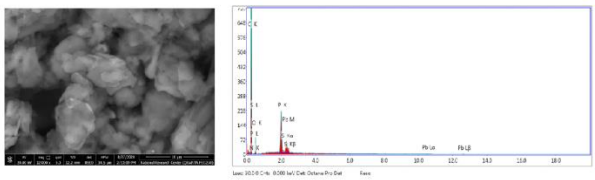

Representative element	Weight %	Atomic %	Net Interactive	Error %
C	75.77	84.49	99.3	8.55
N	0.93	0.89	0.21	99.99
O	13.68	11.46	11.62	15.85
P	5.87	2.54	52.02	4.71
S	1.08	0.45	9.36	16.58
Pb	2.65	0.17	8.97	17.88

Fig. 5 SEM-EDX of membrane films containing 2.0% Pb-CFT, 49.0% Graphite and 49.0% TCP; with a total weight 20 mg.

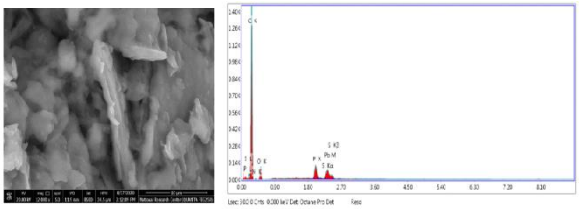

Representative element	Weight %	Atomic %	Net Interactive	Error %
C	78.65	85.56	193.82	6.46
N	2.70	2.52	0.82	38.82
O	12.77	10.43	14.50	15.23
P	2.23	0.94	27.30	8.65
S	0.92	0.38	11.48	14.18
Pb	2.73	0.17	13.16	16.14

Fig. 6 SEM-EDX of membrane films containing 2.0% Pb-CFT, 48.5% Graphite, 48.5% TCP and 1.0% MWCNTs; with a total weight 20 mg.

Calibration graphs were constructed for the three different electrodes, Fig. 7. The results showed good improvement in the electrode response from the electrode (a) to (c) in terms of the application range, slope, and detection limit which is a good agreement SEM and EDX data, Fig. 7.

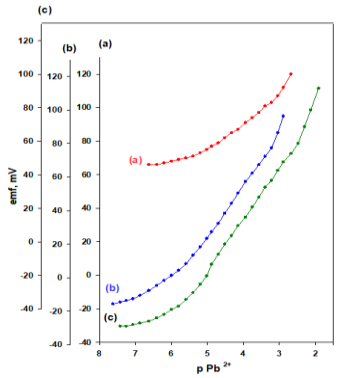

Fig. 7 Calibration graphs for electrode (a) unmodified arbon paste electrode 50.0% Graphite + 50% TCP, (b) 2.0% Pb-CFT+49.0% Graphite+49.0% TCP and (c) 2.0% Pb-CFT + 48.5% graphite + 48.5% TCP +1% MWCNT.

3.10. New criteria of banknote withdrawal from circulation

Banknotes can be subjected during their lifetime in circulation to soiling only, deterioration, or both at the same time (known as aging). Central banks are responsible for the withdrawal of banknotes and defining the criteria upon which the withdrawal occurs. In this part, we are studying the relation between the main three reasons of withdrawal and Pb(II) concentration which were found to be accumulated on the surface of the banknote paper during circulation.

Banknote wear can be biological or non-biological [59]. Physical reasons are divided into chemical, thermal, and electromagnetic, causing two phenomena to appear: soiling and deterioration. Non-biological contact and soiling are the main reasons for the accumulation of metal ions on the banknote since high amounts of heavy metals are present in waste banknote paper [29].

Soiling of banknote is the change in color due to the accumulation of soils during the banknote lifetime. One of the main reasons for soiling is the human sebum that accumulates on the banknote's surface due to finger contact, leaving fingerprints on the banknote surface over time and forming yellow sebum, 99% water, and 1% solids. The best method to recognize soiling on banknotes is based on optical measurements. As a result of banknote circulation, adsorption of soils, dust, and metal ions from the sorting equipment, cash machines, and coins occur, which causes weakening of cotton fiber [60].

Deterioration of banknotes is caused mainly by changing the humidity level, where high humidity causes an elongation of cellulose fibers, making it wavy. Also, it accelerates the growth of microscopic *fungi* and *Molds*. On the other hand, the low humidity causes an irreversible loss of structurally bound water in notes, causing the paper to dry out, lose elasticity, and become brittle. When the fibers become weak, the circulation causes a decrease in the stiffness of note (Limpness). As a result of the circulation, humidity accelerates the accumulation of soils, dust, and metal ions.

When the banknote paper is subjected to both soiling and deterioration, a new phenomenon is generated called aging. Plain porosity is the best term to express this phenomenon, as the increase in porosity reflects the increase in pores between fibers due to the aging of the banknote paper. The term plain porosity refers to the airflow through the banknote paper. The higher the airflow, the more spaces between fibers [60].

The present study classified the fitness levels according to the three parameters of withdrawal, soiling, deterioration, and aging, measured in Table 6. The results indicated that the brightness decreases with circulation, which is attributed to surface soiling of the banknote paper due to the accumulation of dust, metal ions, and sweat droplets from fingerprints on the paper surface.

Table 6. Banknote's lead concentration and the fitness level according to soiling, deterioration, and aging criteria.

Fitness Level	Lead concentration (mg/L)	Soiling	Deterioration	Aging
		Brightness %	Stiffness (mN)	Porosity (mL/min.)
New banknote	0.0	72.0	53.1	2.0
1	1.80	65.3	48.6	11.4
2	-	55.1	33.4	14.3
3	5.73	45.5	22.3	27.7
4	-	35.3	17.3	72.3
5	7.45	22.0	12.4	214.1

By that time, the volatile components evaporate and become more viscous and almost solids [60]. The stiffness decreases with circulation as the banknote fibers become weak and the bonding between fibers breaks, causing them to become brittle.

On the other hand, the porosity increases with circulation, and it becomes severe at fitness level 5 (214.1 ml/min.). This is due to expanded pores between cotton fibers in banknote paper. Crumpling in circulation causes the fillers in the banknote paper to fill out, which is responsible for connecting the fibers net and preventing the penetration of the soil to the banknote paper. As a result, soils and metal ions are accumulated on the surface and between fibers causing the banknote paper to become weak and brittle [61].

The present study was extended to investigate the population of fitness levels of the three main withdrawal criteria in circulation to find the fitness level at which the withdrawal takes place for each of them. Figure 8 showed that in the case of soiling, the population in circulation increased from new uncirculated banknote (2.0 %) to fitness level 4 (25.0%) and decreased in fitness level 5 (13.1%), which indicates that the withdrawal occurs in fitness level 5. At the same time, in case of deterioration, the population increased from new uncirculated banknote (2.0 %) to fitness level 4 (22.9%), then it decreased at fitness level 5 (21.0%).

For aging, the population in circulation increased from new uncirculated banknote (1.5%) to fitness level 4 (47.7) and decreased in fitness level 5 to (7.2%), which indicates that the withdrawal occurs in fitness level 5.

For measuring the lead concentration, Table 6 indicated that new banknote papers are lead-free, and the lead concentration increases in the banknote with circulation. The results show a good agreement with the withdrawal criteria of banknotes based on soiling, deterioration, and aging. The present results can be considered a new criterion, health criteria, for banknote withdrawal using the proposed electrode, Pb-CFT, for lead concentration measurement.

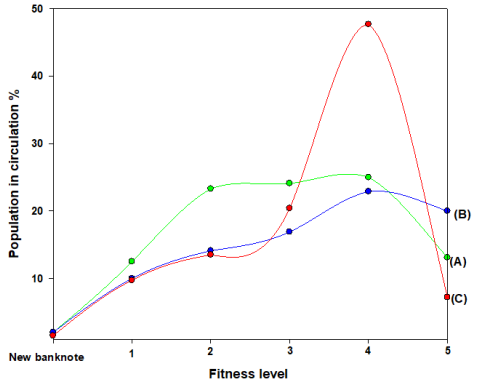

Fig. 8 The population in circulation according to soiling (A), deterioration (B) and aging (C).

3.11. Molecular orbital treatment

3.11.1. The geometry of Ceftriaxone compound

The geometrical structure of Ceftriaxone was optimized at the B3LYP/6-311G** level, and the results are shown in Table 7 and Fig. 9. Ceftriaxone compound has a non-planar configuration. This can be indicated from the dihedral angles, far from 0° or 180°. This also can be verified from the bond angel (<C28-C25-C18), which has a value of 124.240 °, Table 7.

Table 7. Selected geometric bond lengths, bond angles, and dihedral angles of the optimized Ceftriaxone using B3LYP/6-311G**

Bond lengths (Å)		Bond angles		Dihedral angles	
N31-C29	1.373	N31-C29-N28	124.240	N31-C29-N28-C25	-176.641
C29-S27	1.775	N31-C29-S27	120.973	C29-N28-C25-C18	-179.911
S27-C26	1.738	C29-S27-C26	88.171	C29-N28-C25-C26	-0.599
C26-C25	1.367	S27-C26-C25	110.301	N28-C25-C26-S27	0.955
C26-N28	1.3855	C26-C25-N28	115.519	N31-C29-S27-C26	177.202
N28-C29	1.292	C26-C25-C18	126.284		
C18-C25	1.478	C25-C18-C15	118.145		

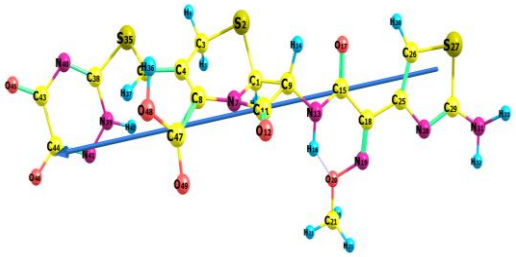

Fig. 9 Optimized geometry, numbering system and vector of dipole moment of Ceftriaxone using B3LYP/ 6-311G**.

3.11.2. Ground-state properties and global reactivity descriptors

It was found that the energy difference between the HOMO and LUMO, Ceftriaxone, E_g occurs at 1.17 eV. The energy gap for the compound is a minimum (1.17 eV) value so, the charge transfer and polarization can occur quickly with more reactivity within this compound. Calculations of the electronegativity, χ, global softness, S, chemical potential, π, chemical hardness, η, were done using LUMO and HOMO energies and recorded in Table 8 and Fig. 10. The compound has low η and S valuesmeaning , that the charge transfer occurs quickly and has a lower chemical hardness. It can be decided that the small E_g gap designates a softness and reactive molecule. The electron affinity value is 4.6956. The processed reactivity parameters shown in Also Table 8 reveal that the compound has low η and minimum S values, indicating lower chemical hardness. The 3-D distribution of frontier MOs, HOMO, and LUMO of Ceftriaxone is presented in Fig. 10. The calculated values of E_{HOMO} and E_{LUMO} of Ceftriaxone are -0.2157 and -0.1726 au, respectively; thus, the energy gap value E_g is 1.1725 eV.

It can be concluded from the molecular orbital diagrams in Fig. 10 that the HOMO and LUMO of Ceftriaxone are mainly allocated over half of the molecule. Table 8 and Fig. 10 shows the partial frontier molecular orbital compositions and the energy levels of Ceftriaxone in the ground state.

3.11.3. Non-linear optical properties (NLO)

The circulation of the atomic charges in the chelates is valuable in determining the magnitude and direction of the moment vector as well, which depends on the centers of both positive and negative charges. The anisotropy of the polarizability, the mean polarizability, the dipole moment, and the first order hyperpolarizability were calculated for Ceftriaxone using the same level. The obtained values and the experimental values of urea are tabulated in Table 9. The considered dipole moment value of Ceftriaxone in the gas phase is 16.2537 D. The analyzed value of the polarizability of Ceftriaxone has a value of 15.1783×10^{-24} (esu). The studied Ceftriaxone is high polarizability and first order hyperpolarizability compared with urea [62] as a prototype substance. The polarizabilities and first order hyperpolarizabilities are reported in atomic units (a.u.), the calculated values have been changed into electrostatic units (esu) using a conversion factor of 0.1482×10^{-24} esu for α and 8.6393×10^{-33} esu for β, where urea is used as a standard example in non-linear optical studies which in this study is chosen as reference material as there were no experimental values of NLO properties of the studied compound. The extent of the molecular hyperpolarizability (<β>) is critical in the non-linear optical system. The calculated (<β>) value examination shows that Ceftriaxone is 107 times greater than Urea.

Table 8. The total energy of HOMO and LUMO, energy gap, ionization energy (I, eV), electron affinity (A, eV), absolute electronegativities, (χ, eV), absolute hardness (η, eV), global softness (S, eV^{-1}, chemical potential (π, eV^{-1}) global electrophilicity (***ω***, eV), additional electronic charge, $\Delta N_{max,}$ of Ceftriaxone using B3LYP/6-311G**

E_T, a.u.	E_{HOMO}, a.u.	E_{LUMO}, a.u.	Eg, eV	I, eV	A, eV	χ, eV	η, eV	S, eV	π ες	ω, eV	$\Delta N_{max.}$
-2815.7	-0.2157	-0.1726	1.1725	5.8681	4.6956	5.2819	0.5863	0.8528	-5.2819	23.7919	9.0089

Therefore, the studied compound reveals considerable polarizability and first order hyperpolarizability and is projected to be successfully encouraged for NLO materials.

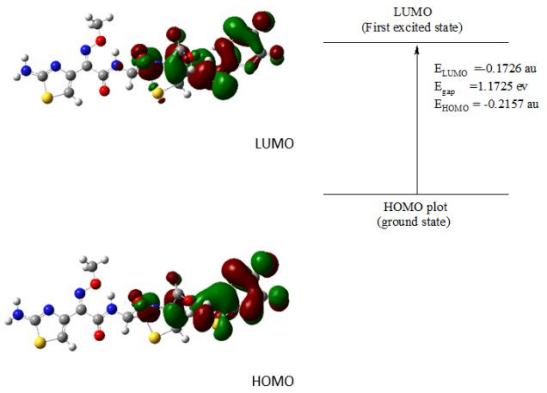

Fig. 10 HOMO and LUMO charge density maps of the studied Ceftriaxone using B3LYP/6-311G** level.

3.11.4. Molecular electrostatic potential (MEP)

The nucleophilic and electrophilic effect and hydrogen bonding associated with any molecular system can be elucidated in terms of the natural charges and charge transfer on active sites of the studied compound [63]. The increasing potential is following the order: red < orange < yellow < green < blue [64, 65]. The calculated 3D MEP maps of the Ceftriaxone are analyzed from the optimized structure using B3LYP/6-311G** and presented in Fig. 11. The result shows that the negative region (red) is mainly over the O46 and O45 atomic sites which are caused by the contribution of lone-pair electrons of oxygen atoms. Moreover, the positive (blue) potential sites are round the carbon and hydrogen atoms, while other carbon atoms seem to have zero potential. Attending to the molecule with negative electrostatic potential will be exposed to electrophilic attack, the more negative, the higher the shift towards electrophilic attack.

Table 9. Calculated total static dipole moment (μ), the mean polarizability <α>, anisotropy of the polarizability Δα and the first-order hyperpolarizability <β > configuration for the studied Ceftriaxone using B3LYP/6-311G

Property	Urea	Ceftriaxone
μ, D	1.3197	16.2537
αxx, a.u.	-	-328.7053
αyy	-	-226.6811
αzz	-	-225.8991
αxy	-	-38.4516
αxz	-	-1.9316
αyz	-	-11.3749
<α> esu	-	-3.8596×10^{-23}
Δα, esu	-	15.1783×10^{-24}
βxxx	-	-2304.6327
βxxy	-	-66.4192
βxyy	-	-141.5906
βyyy	-	40.2007
βxxz	-	166.9164
βxyz	-	25.048
βyyz	-	-10.5583
βxzz	-	45.7178
βyzz	-	-17.6018
βzzz	-	-21.6981
<β>, esu	0.1947×10^{-30}	20.7750×10^{-30}

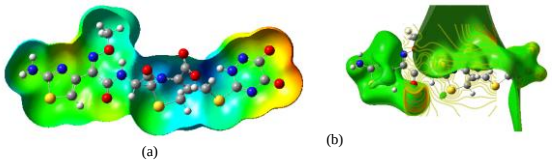

Fig. 11 Molecular electrostatic potential (a) and contour electrostatic potential (b) surfaces of Ceftriaxone using B3LYP/6-311G**.

4. Conclusion

A modified carbon paste electrode was constructed for Pb(II) determination. It is characterized by a reasonable long-term stability, relatively fast response, good sensitivity, and responsive potential stability.

Most of the metal ions do not affect the selectivity for Pb(II) ions of the constructed electrode. The surface morphology studies of the electrode using SEM and EDX showed a good agreement with the modified electrode's calibration graphs compared with the unmodified one. A new way for banknote withdrawal from circulation to measure the lead concentration using the proposed electrode was developed. The results showed a good agreement between the banknote life cycle, the conventional withdrawal criteria (aging, soiling, and deterioration), and the Pb(II) concertation. Quantum mechanical calculations explained the type of bond in the newly prepared compound and HOMO and LUMO were used to explain the charge transfer within this compound.

5. Conflicts of interest

In accordance with our policy on Conflict of interest please ensure that a conflicts of interest statement is included in your manuscript here. Please note that this statement is required for all submitted manuscripts. If no conflicts exist, please state that "There are no conflicts to declare".

6. Acknowledgments

Collate acknowledgments in a separate section at the end of the article before the references and do not, therefore, include them on the title page, as a footnote to the title or otherwise. List here those individuals who provided help during the research (e.g., providing language help, writing assistance or proof reading the article, etc.).

7. References

[1] Ganjali M.R., Khoshsfar H., Sherzadmehr A., Javanbakht M. and Faridbod F., Improvement of Carbon Paste Ion Selective Electrode Response by Using Room Temperature Ionic Liquids (RTILs) and Multi-Walled Carbon Nanotubes (MWCNTs). International Journal of Electrochemical Science, 4, 435-443 (2009).

[2] Youssef A.F.A., Abd Dayiem M. and Shehab O.R., Use of dicloxacillin Al (III) Complex as a modifier for determination of Al (III) ion in real samples. Electroanalysis, 32, 2902-2912 (2020).

[3] Arvand M. and Kermanian M., Potentiometric Determination of Aluminum in Foods, Pharmaceuticals, and Alloys by AlMCM-41-Modified Carbon Paste Electrode. Food Analytical Methods, 6, 578-586 (2013).

[4] Heidaria Z. and Masrourniaa M., A Novel Modified Carbon Paste Electrode for the Determination of Chromium(III) in Water. Journal of Analytical Chemistry, 73, 824-831 (2018).

[5] Ghalkhani M., Ghelichkhani F. and Ghorbani-Bidkorbeh F., Study and Optimization of The Necessary Conditions for The Sensitive Determination of The Lead Ion by a Modified Carbon Paste Electrode in Environmental Water Samples. Iranian Journal of Pharmaceutical Research, 17, 44-53 (2018).

[6] Abdallah N.A., Carbon Nanotube Electrodes in Comparison to Coated Platinum Wire and Carbon Paste Selective Electrodes for the Determination of Tramadol Hydrochloride in Bulk, Pharmaceutical Formulations, and Spiked Human Plasma and Urine. Sensors and Materials, 28, 797-816 (2016).

[7] Hyalij R.R., Bhagure G.R. and Chavan R.P., Development of Electrochemical Sensor for Determination of Lead (II) Ion. International journal of chemical studies, 5, 745-750 (2017).

[8] Njatia S.Y. and Magutab M.M., Lead-based paints and children's PVC toys are potential sources of domestic lead poisoning - A review. Environmental Pollution, 249, 1091-1105 (2019) .

[9] Saritha B., Giri A. and Reddy T.S., Direct spectrophotometric determination of Pb (II) in alloy, biological and water samples using 5-bromo-2-hydroxyl -3- methoxybenzaldehyde-4-hydroxy benzoichydrazone. Journal of Chemical and Pharmaceutical Research, 6, 1571-1576 (2014).

[10] Jankiewicz B., Ptaszyński B. and Wieczorek M., Spectrophotometric Determination of Lead in the Soil of Allotment Gardens in Łódź. Polish Journal of Environmental Studies, 10, 123-126 (2001).

[11] Dadfarnia S., Shabani A.M.H. and Shirie H.D., Determination of lead in different samples by atomic absorption spectrometry after preconcentration with dithizone immobilized on surfactant-coated alumina. Bulletin of the Korean Chemical Society, 23, 545-548 (2002).

[12] Cho H.J. and Myung S.W., Determination of cadmium. Chromium and lead in polymers by ICP-OES using High Pressure Asher (HPA). Bulletin of the Korean Chemical Society, 32, 489-497 (2011).

[13] Shirkhanloo H., Sedighi K. and Mousavi H.Z., Determination of Trace Amount of Lead in Industrial and Municipal Effluent Water Samples Based on Dispersive Liquid-Liquid Extraction. Journal of the mexican chemical society, 58, 137-141 (2014).

[14] Cammann K., Robecke M. and Beumer J., Fresenius. Simultaneous determination of organic ionic lead and mercury species using HPLC. Journal of Analytical Chemistry, 350, 30-33 (1994).

[15] Zapata-Flores E.D.J., Gazcón-Orta N.E. and Flores-Vélez L.M., A direct method for the determination of lead in beers by differential pulse polarography-anodic stripping voltammetry. Journal of Materials and Environmental Science, 7, 4467-4470 (2016).

[16] Guo J., Chai Y., Yuan R., Song Z. and Zou Z., Lead (II) carbon paste electrode based on

derivatized multi-walled carbon nanotubes: Application to lead content determination in environmental samples. Sensors and Actuators B, 155, 639-645 (2011).
[17] RezaGanjali M.R, Motakef-Kazami N., Faridbod F. and Norouzi S.P., Determination of Pb2+ ions by a modified carbon paste electrode based on multi-walled carbon nanotubes (MWCNTs) and nanosilica. Journal of hazardous materials, 173, 415-419 (2010).
[18] Ghaedi M., Jaberi S.Y.S., Hajati S., Montazerozohori M., Asfaram A. and Zareh M., Modified Carbon Paste Electrode for Pb2+ Ion Determination: Response Surface Methodology. IEEE Sensors Journal, 15, 2974-2983 (2015).
[19] Ghaedi M., Shokrollahi A., Montazerozohori M., Mansouri M., Khodadoust S., Mousavi A. and Hossainian H., Influence of Multiwalled Carbon Paste Nanotubes on Response of Pb2+ Ion Selective Carbon Paste Electrode Based on 2-((6-(5-Bromo-2-Hydroxybenzylideneamino) Hexylimino) Methyl)-4 Bromophenol as Novel Neutral Carrier. IEEE Sensors Journal, 1, 2449-2457 (2011).
[20] Saadeh S.M., Abu-Shawish H.M., Abed-Almonem K., Abu Mkhada A. and Safi W., A new potentiometric thiosalicylamide-functionalized polysiloxane carbon paste electrode for lead(II) determination. Journal of Electroanalytical Chemistry, 687, 11-17 (2012).
[21] Bagheri M., Yari A. and Mahdipoor. A., Determination of lead ion by a modified carbon paste electrode based on multi-walled carbon nanotubes (MWCNTs) and poly 4-N-pyridine para styrene sulfonamide. Journal of Environmental Treatment Techniques, 6, 53-58 (2018).
[22] Zayed M.A., Mahmoud W.H., Abbas A.A., Ali A.E. and Mohamed G.G., A highly sensitive, selective and renewable carbon paste electrode based on a unique acyclic diamide ionophore for the potentiometric determination of lead ions in polluted water samples. RSC Adv., 10, 17552-17560 (2020).
[23] Zhad H.R.L.Z., Aboufazeli F., Amani V., Najafi E., and Sadeghi O., Modification of Multiwalled Carbon Nanotubes by Dipyridile Amine for Potentiometric Determination of Lead(II) Ions in Environmental Samples. Journal of Chemistry, 2013, 1-7 (2012).
[24] Mashhadizadeh M.H., Khani H., Shockravi A. and Sadeghpour M., Determination of ultratrace levels of lead (II) in water samples using a modified carbon paste electrode based on a new podand. Materials Science and Engineering: C 31, 1674-1680 (2011).
[25] Afkhami A., Shirzadmehr A., Madrakian T. and Bagheri H., Improvement in the performance of a Pb2+ selective potentiometric sensor using modified core/shell SiO2/Fe3O4 nano-structure. Journal of Molecular Liquids, 199, 108-114 (2014).
[26] Bagheri M., Talaiekhozani A. and Ahmadvand F., Determination of Lead Ion by a Modified Carbon Paste Electrode Based on Multi-Walled Carbon Nanotubes (MWCNTs) and Ligand (N-(4-Hydroxyphenyl) Ethanamide). Iranian Journal of Health, Safety & Environment, 2, 243-249 (2015).
[27] Guo J., Chai Y., Yuan R., Song Z. and Zou Z., Lead (II) carbon paste electrode based on derivatized multi-walled carbon nanotubes: Application to lead content determination in environmental samples. Sensors and Actuators B, 155, 639-645 (2011).
[28] Khan Y., Roy M., Rawal R.K. and Bansal U.K., A Review-Ceftriaxone for Life. Asian Journal of Pharmaceutical Research, 7, 35-48 (2017).
[29] Aghmashhadi O.Y., Asadpour G., Garmaroody E.R., Zabihzadeh M., Rocha-Meneses L. and Kikas T., The Effect of Deinking Process on Bioethanol Production from Waste Banknote Paper. Processes, 8, 1-20 (2020).
[30] Welcher F.J., Analytical uses of ethylenediaminetetraacetic acid, Van Nostrand, 1967.
[31] Ahmad A., Mohammad A., Synthesis and Characterization of Silver Oxide Nanoparticles by a Novel Method. International Journal of Scientific Engineering and Research (IJSER), 4, 2229-5518 (2013).
[32] Rassi S.F., Chemically modified carbon paste ion-selective electrodes for determination of atorvastatin calcium in pharmaceutical preparations. Journal of Analytical Chemistry, 12, 65-73 (2017).
[33] Li X., Maa X. and Huang M., Lead(II) ion-selective electrode based on polyaminoanthraquinone particles with intrinsic conductivity. Talanta, 78, 498-505 (2009).
[34] Gadzekpo V.P.Y. and Christian G.D., Determination of selectivity coefficients of ions selective electrodes by a matched potential method. Analytica Chimica Acta, 164, 279-282 (1984).
[35] Umezawa Y., Umezawa K., Buhlmann P., Hamada N., Aoki H., Nakanishi J., Sato M., Xiao K.P. and Nishimura Y., Potentiometric selectivity coefficients of Ion-selective electrodes part II. Inorganic anions. Pure and Applied Chemistry, 74, 923-994 (2002).
[36] Baumann E.W., Trace fluoride determination with specific ion electrode. Analytica Chimica Acta, 42, 127-132 (1968).
[37] APHA (American Public Health Association), AWWA (American Water Works Association), and WEF (Water Environment Federation). 2017. Standard Methods for the Examination of Water and Wastewater, 23rd ed. (Rice, E. W., Baird, R. B., Eaton, A. D., Clesceri, L. S. eds.) Washington DC.
[38] Frisch M.J., Trucks G.W., Schlegel H.B., Scuseria G.E., Robb M.A., Cheeseman J.R., Scalmani G., Barone V., Mennucci B., Petersson G.A., Nakatsuji H., Caricato M., Li X., Hratchian H.P., Izmaylov A.F., Bloino J., Zheng G., Sonnenberg J.L., Hada M., Ehara M., Toyota K., Fukuda R., Hasegawa J., Ishida M., Nakajima T., Honda Y., Kitao O., Nakai H., Vreven T., Montgomery J.A. Jr., Peralta J.E., Ogliaro F., Bearpark M., Heyd J.J., E., Brothers K.N. Kudin, Staroverov V.N., Kobayashi R., Normand J., Raghavachari K., Rendell A., Burant J.C., Iyengar

S.S., Tomasi J., Cossi M., Rega N., Millam J.M., Klene M., Knox J.E., Cross J.B., Bakken V., Adamo C., Jaramillo J., Gomperts R., Stratmann R.E., Yazyev O., Austin A.J., Cammi R., Pomelli C., Ochterski J.W., Martin R.L., Morokuma K., Zakrzewski V.G., Voth G.A., Salvador P., Dannenberg J.J., Dapprich S., Daniels A.D., Farkas O., Foresman J.B., Ortiz J.V., Cioslowski J. and Fox D.J., Gaussian Inc., Wallingford, CT. 2009.

[39] Becke A.D., Density-functional thermochemistry. III. The role of exact exchange. The Journal of Chemical Physics, 98, 5648-5652 (1993).

[40] Lee C., Yang W.T. and Parr R.G., Development of the Colle-Salvetti correlation-energy formula into a functional of the electron density. Physical Review B - Condensed Matter and Materials Physics, 37, 785-789 (1988).

[41] Frisch M.J., Pople J.A. and Binkley J.S., Self-consistent molecular orbital methods 25. Supplementary functions for Gaussian basis sets. The Journal of Chemical Physics, 80, 3265-3269 (1984).

[42] Dennington R., Keith T. and Millam J., Gauss View Version 5, Semichem Inc. Shawnee Mission (2009).

[43] El Ghamaz N.A., Diab M.A., El Bindary A.A., El Sonbati A.Z. and Seyam H.A., Geometrical structure and optical properties of antipyrine Schiff base derivatives. Materials Science in Semiconductor Processing, 27, 521-531 (2014).

[44] El-Sonbati A.Z., Diab M.A., El Bindary A.A. and Morgan Sh.M., Supramolecular spectroscopic and thermal studies of azodye complexes. Spectrochimica Acta, part A: Molecular and Biomolecular Spectroscop, 127, 310-328 (2014).

[45] Chocholoušová J., Špirko V. and Hobza P., First local minimum of the formic acid dimer exhibits simultaneously red-shifted O-H···O and improper blue-shifted C-H···O hydrogen bonds. Physical Chemistry Chemical Physics, 6, 37-41 (2004).

[46] Avci D., Second and third-order nonlinear optical properties and molecular parameters of azo chromophores: Semiempirical analysis. Spectrochimica Acta Part A: Molecular and Biomolecular Spectroscopy, 82, 37-43 (2011).

[47] Avci D., Başoğlu A. and Atalay Y., Ab initio HF and DFT calculations on an organic non-linear optical material. Structural Chemistry, 21, 213-219 (2010).

[48] Avci D., Cömert H. and Atalay Y., Ab initio Hartree-Fock calculations on linear and second-order nonlinear optical properties of new acridine-benzothiazolylamine chromophores. Journal of Molecular Modeling, 14 ,161-169 (2008).

[49] Issa Y.M., Ibrahim H., El-Rhazi M. and Shehab O.R., Nanotechnol. Determination of Lead in Some Environmental Samples Using Chemically Modified Carbon Paste Electrode Based on Lead. Tetrakis(Imidazolyl)Borate. Journal of Nanoscience Letters, 5, 392-401 (2013).

[50] Svancara I., Vytras K., Barek J. and Zima J., Carbon paste electrodes in modern electroanalysis. Critical Reviews in Analytical Chemistry, 31, 311-345 (2001).

[51] Singh A.K. and Mehtab S., Calcium(II)-selective potentiometric sensor based on α-furildioxime as neutral carrier. Sensors and Actuators B, 123, 429-436 (2007).

[52] Oesch V., Ammann D. and Simon W., Ion-selective membrane electrodes for clinical use. Clinical Chemistry, 32, 1448-1459 (1986).

[53] Bard A.J., Parson R. and Jordan J., Standard potentials in aqueous solution, Marcel Dekker, Inc. 1985.

[54] Sun C.Q., Sun Y.P., Zhang X., Xu H.D. and Shen J.C., Selective potentiometric determination of copper (II) ions by use of a molecular deposition film electrode based on water-soluble copper phthalocyanine. Analytica Chimica Acta, 312, 207-212 (1995).

[55] Saleh M.B., Copper (II) Sensor Based on a Cephaloridine Antibiotic PVC Matrix. Analytical Letters, 33, 1501-1512 (2008).

[56] Marinho-Reis A.P., Costa C., Rocha F., Cave M., Wragg J., Valente T., Sequeira-Braga A. and Noack Y., Biogeochemistry of Household Dust Samples Collected from Private Homes of a Portuguese Industrial City. Geoscience, 10, 1-21 (2020).

[57] Antropov L.I., Theoretical Electrochemistry, Mir Publisher, Moscow 1972.

[58] Fang Z., Xu S. and Zhang S., The determination of trace amounts of heavy metals in waters by a flow-injection system including ion-exchange preconcentration and flame atomic absorption spectrometric detection. Analytica Chimica Acta, 164, 41-50 (1984).

[59] Kyrychok T., Shevchuk A., Nesterenko V. and Kyrychok P., Banknote deterioration, Banknote Paper Deterioration Factors: Circulation Simulator Method. Bioresources, 9, 710-724 (2014).

[60] Boutin G.E., $1 Circulation Field study, U. S. Bureau of Engraving and Printing. Currency Conference, Praque, 2008.

[61] Scruton B., The deposition of Fingerprint films. Journal of Physics D: Applied Physics, 8, 714-723 (1975).

[62] Lin Y.Y., Rajesh N.P., Raghavan P.S., Ramasamy P. and Huang Y.C. Materials Letters, 56, 1074-1077 (2002).

[63] Scrocco E. and Tomasi J., Electronic molecular structure, reactivity, and intermolecular forces: an euristic interpretation by means of electrostatic molecular potentials. Advances in Quantum Chemistry, 11, 115-193 (1978).

[64] Politzer P. and Murray J.S., The fundamental nature and role of the electrostatic potential in atoms and molecules. Theoretical Chemistry Accounts, 108, 134-142 (2002).

[65] Sajan D., Joseph L., Vijayan N. and Karabacak M., Natural bond orbital analysis, electronic structure, non-linear properties, and vibrational spectral analysis of l -histidinium bromide monohydrate: a density functional theory. Spectrochimica Acta, Part A, 81, 85-98 (2011).